Could WAG be the Right EOR Process for Libyan Carbonate Reservoirs?

Rafa Labedi, Omar Abdulkarim, Karlo Krizmanic and Saleh El-Fakhri*

هل تعاقب الماء بالغاز عملية إسترداد صحية بمكامن الصخور الكلسية بليبيا؟

رافع اللبيدي، عمر عبد الكريم، كارلو كريزمانيك وصالح الفاخري

كميات كبيرة من النفط الخام ستبقى غير مستخلصة من مكمن الصخور الكلسية المنتجة بطريقة الغمر بالماء من وحدة النافورة – أوجلة أحد الحقول العملاقة التابعة الشركة الخليج العربي النفط، نقدم في هذه الورقة أهمية الدراسات المعملية ومعرفة البحث التقني كجزء رئيسي من إنجاز دراسات المحاكاة المتكاملة لتقييم المسترد الإضافي من الناحية التقنية والجدوى الاقتصادية والتخطيط تعتبر نتائج تحاليل اللب المتقدمة أحد الأدوات القوية لمعايرة النماذج المكمنية، ومن أجل تشريق خواص المائع وخاصة الابتلالية ونهاية نقاط التشبع، تجري التجارب عند ظروف المكمن الحقيقية.

دلت تجارب كثافة الاستنفاذ لثاني أكسيد الكربون على الاختراق المبكر لثاني أكسيد الكربون وانخفاض في كفاءة الإزاحة بينما نتج عن اختبارات الإزاحة بطريقة تعاقب الماء بالغاز غير الممتزج استخلاص زيت عالى، وكما هو الحال في الأنبوب الرفيع عند الضغط الأدنى للإمتزاجية.

إذا طريقة تعاقب الماء بالغاز غير الممتزج بمقدرتها العمل أفضل عند أي عملية حقن للغاز غير الممتزج باستخدام الغاز الهيدروكربوني والنيتروجين أو غازات الاحتراق عند ضغوطات منخفضة للغاية بدلا من الضغط الأدنى للإمتز اجية بمكامن جيرية ذات بيئات ترسيب متشابهة وتغير في نشأة النسيج وانتقائية في الإذابة.

Abstract: In Nafoora Augila Unit (NAU), one of the giant oil fields of AGOCO, an appreciable amount of oil will remain unrecoverable in the prolific carbonate layers after waterflooding. In this paper, we present the importance of experimental studies and knowledge (technological research) as a major part of achieving integrated simulation studies for evaluating the EOR technical and economical feasibility, and planning. The special core analysis (SCAL) results are one of the most powerful tools to calibrate reservoir models. The laboratory experiments are performed at actual reservoir conditions to honor fluid properties, the wettability

and saturation end-points. CO_2 gravity drainage experiments resulted in an early CO_2 breakthrough and low displacement efficiency, while immiscible water alternating gas (IWAG) displacement tests resulted in an oil recovery as high as in case of slim tube, at the minimum miscibility pressure (MMP). Therefore, IWAG could potentially work well for any other immiscible gas injection process using hydrocarbon gas, nitrogen, or fuel gases, and at significantly lower pressures than the MMP in carbonate reservoirs of similar depositional environment and diagenetic fabric selective dissolution.

INTRODUCTION

The common classification of WAG processes is to distinguish between miscible, MWAG, and

^{*} Arabian Gulf Oil Company (AGOCO), Benghazi, Libya.

immiscible, IMWAG displacements. Because of failure to maintain sufficient pressure, real field cases may oscillate between MWAG and IMWAG during the implementation of the WAG process. Important technical factors affecting WAG performance have been identified: heterogeneity, wettability, fluid properties, miscibility conditions, injection techniques, WAG parameters, and physical dispersion and flow geometry.

The oil recovery can be described by three contributions: microscopic displacement efficiency, horizontal and vertical sweep efficiencies. Our concern is to highlight aspects of microscopic displacement efficiency in IWAG process by integrations of previous SCAL studies and technological research.

When performing a miscible gas displacement, the residual oil saturation will tend to go toward zero in the flooded area. A problem in MWAG process is that injected water blocks contacts between injected gas and remaining oil. This reduces microscopic displacement efficiency, resulting in higher residual oil saturation. This effect has been found to be a strong function of rock wettability and oil recovery is adversely affected by the presence of mobile water in water-wet cases, but the effect of mobile water is almost negligible in mixed-wet and preferentially oil-wet reservoirs^[1,2,3].

With IWAG process the residual oil saturation after gas-flooding is lower than after water-flooding, meaning that gas has a better microscopic displacement efficiency than water. In water swept zones, the residual oil saturation to water-flooding is reduced through the gas entrapment process. The degree of oil saturation reduction and corresponding trapped gas saturation depend on initial gas saturation and wettability. The experiments demonstrate the need to measured the IWAG microscopic displacement efficiency and trapped gas saturation on preserved or wettability restored cores^[4,5,6].

Gas saturation is divided into two contributors, trapped and mobile gas saturations. Trapped gas can be only become remobilized by dissolving in the oil, and the only contributor to gas flow is the free gas saturation. Reduced residual oil saturation increases the oil mobility. For given oil saturation the water saturation is less in WAG injection by the amount of reservoir volume occupied by the trapped gas. As a result the water mobility and therefore water cut must be less for given oil saturation. Reduced permeability of the gas phase can be achieved by alternate

injection of gas and water. Therefore improved microscopic sweep efficiency in three-phase zones of the reservoirs could add benefit from reduction of mobility in IWAG processes.

The displacement mechanism in IWAG process occurs in a three-phase regime, where the cycling nature of the process creates a combination of imbibitions and drainage. Conventional two-phase relative permeability hysteresis models were unable to describe MWAG and IWAG flows in cores and field trials, where gas and water saturations will increase and decrease alternating. This gives special demands for relative permeability for oil, gas and water phases. Recent approach has been designed for WAG injection using cycle dependant oil, water and gas relative permeabilities^[7,8,9].

Therefore the optimum WAG design is different for each reservoir and needs to be determined for specific reservoir and fine tuned for particular area within reservoir^[10,11].

Microscopic displacement efficiency by WAG processes has to be determined from laboratory experiments.

SCAL PROGRAM

Minimum Miscibility Pressure Requirements

Slim tube tests showed that MMP is 270 barg, and that displacement efficiency does not fall sharply below MMP. A significant amount of oil could be recovered at pressures substantially below slim-tube MMP^[11,12,13].

Keeping in mind with principle of economy we have investigated that possibilities incorporating our best knowledge of the state of art technology.

Petrophysical Classes and Pore Space Classification

Reservoir rock is relatively clean bioclastic limestone. The depositional texture is skeletal grainstone and packstone/wackstone. Early consolidation preserved much of primary porosity. Selective dissolution of skeletal debris in the undersaturated zones of the meteoric phreatic environment provided moldic and pinpoint vuggy porosity. Mesovuggy porosity is the main pore type with additional interparticle and variable microporosity^[14,15]. Figure 1 shows CT-SCAN investigations of the internal structure of the whole

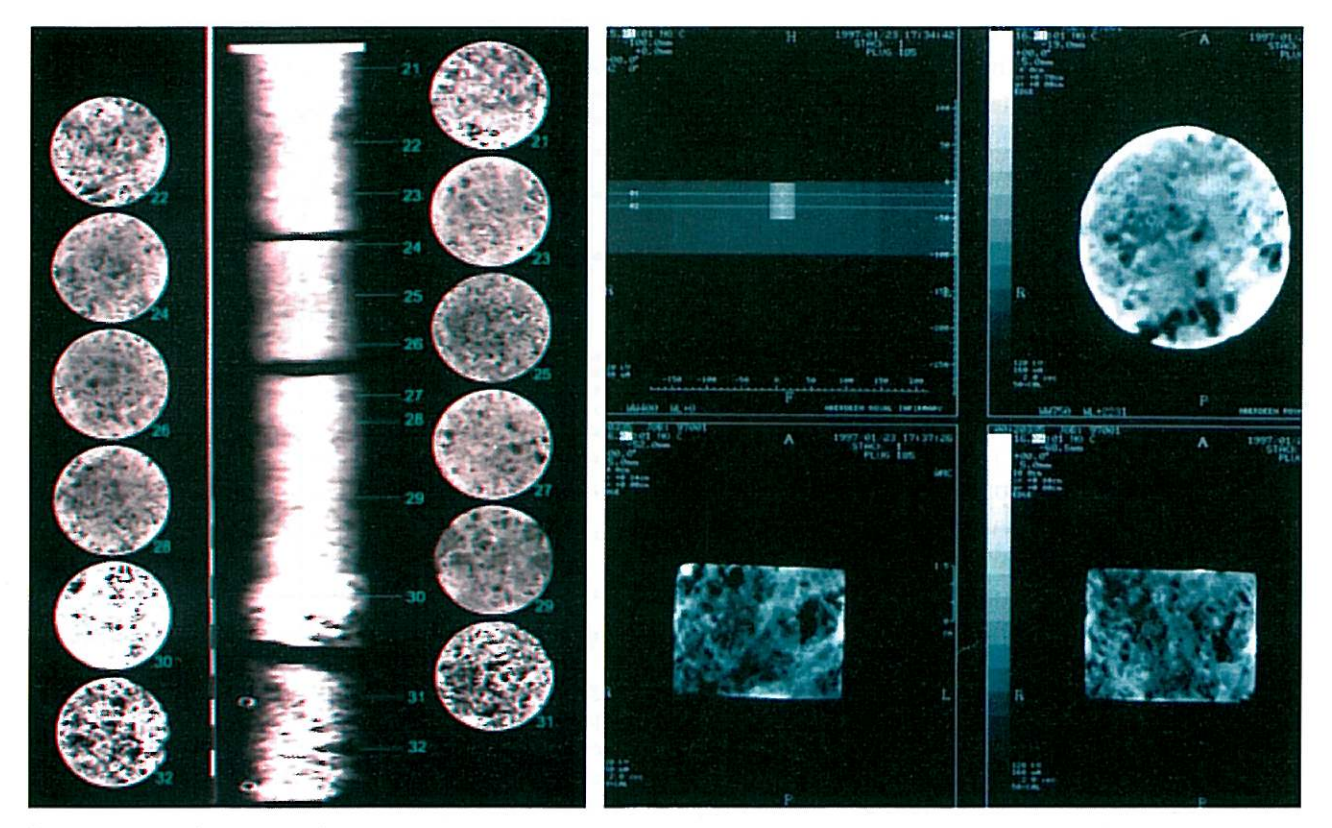


Fig. 1. CT-SCAN images showing pore structure.

core samples. In particular the macroporosity is well visible on most slices.

Rock fabrics has been grouped into four rockfabric petrophysical classes:

- 1. clean coquina limestone dominated by large skeletal grains.
 - 2. skeletal bioclastic grainstone
 - 3. grain dominated packstone/wackstone
 - 4. mud (micritic) dominated limestone

Principal pore types and pore interconnections are grouped into:

- 1. intergranular, macro in rock-fabric class 1, good connected in rock-fabric classes 1 and 2, variably occupied by micritic matrix in rock-fabric classes 2 and 3.
 - 2. secondary dissolution, moldic and vuggy
- 3. good microporosity within micrit materials composed of loosely arranged small calcite crystals (rock-fabric classes 2 and 3).

Pore interconnections in secondary dissolution pore space

- 1. abundant and interconnected touching vuggy porosity and channel like from skeletal and micitic matrix leaching (dominant on 1" and 1.5" small plug scale)
- 2. discrete, separate vuggy porosity (dominant on full diameter and well log scale).

Wettability

The capillary imbibition curves are typical of oilwet samples. The Amott/USBM wettability tests show the reservoir wettability ranges from weak-to-strong oil-wetness^[14,15]. The vuggy system connected by the largest thresholds pore entry radii is strongly oil-wet. The spontaneous imbibitions of water at 80°C for three weeks resulted in the increase of water saturation in the range 8.3% to 9.5%. This is an indication that the majority of intergranular/intercrystalline pore system, variably occupied by micritic matrix, could be less oil wet due to pore structure. Therefore wettability question in intergranular/intercrystalline pore system may be the matter of some concern.

Resistivity Measurements and Interpretation

A.) Use of Maxwell-Garnett Model to Interpret Formation Factor, FF, Measurements.

In heterogeneous carbonate reservoirs the porosity exponent, m, is a major factor of uncertainty in the calculation of fluid saturation. Complex electrical behavior may result from the way in which vuggs are related to each other, and to the intergranular pore space.

FF's were measured on core plugs from two carbonate reservoirs at net overburden pressure, NOB, by simulated formation brine, and reservoir oil[14,15]. CT-SCAN images of core samples were used to characterize pore types and interconnections in secondary dissolution pore space. The Maxwell-Garnett, M-G, model:

$$F_{t} = \frac{1}{\boldsymbol{\Phi}_{i}^{m}} \left[\frac{1 - \boldsymbol{\Phi}_{v} \left(\frac{1 - \boldsymbol{\Phi}_{i}^{m}}{1 - 2\boldsymbol{\Phi}_{i}^{m}} \right)}{1 + 2\boldsymbol{\Phi}_{v} \left(\frac{1 - \boldsymbol{\Phi}_{i}^{m}}{1 + 2\boldsymbol{\Phi}_{i}^{m}} \right)} \right]$$
(1)

allows for better interpretation of FF if both, the intergranular, Φi, and vuggy porosity, Φv, vary independently and simultaneously, resulting in a range of FF for a single total porosity, $\Phi^{[16,17]}$.

Eq. (2) and Eq. (3) are the results of M-G model for abundant, interconnected touching and channel like vuggy poro system, and for discrete and separate vuggy pore system, respectively[18,19].

$$F = 2.3217\Phi^{-1.1619}$$
 $r^2 = 0.8332$ (3)
 $F = 0.4469\Phi^{-2.549}$ $r^2 = 0.8511$ (2)

$$F = 0.4469\Phi^{-2.549} \qquad r^2 = 0.8511 \tag{2}$$

Intercept a, known as tortuosity parameter, could be related to depositional environments and diagenetic fabric-selective dissolution process. Figures 2 a and b are the application of M-G model to interpretation of FF-Φrelationships, and division of total porosity into matrix and vuggy[18,19].

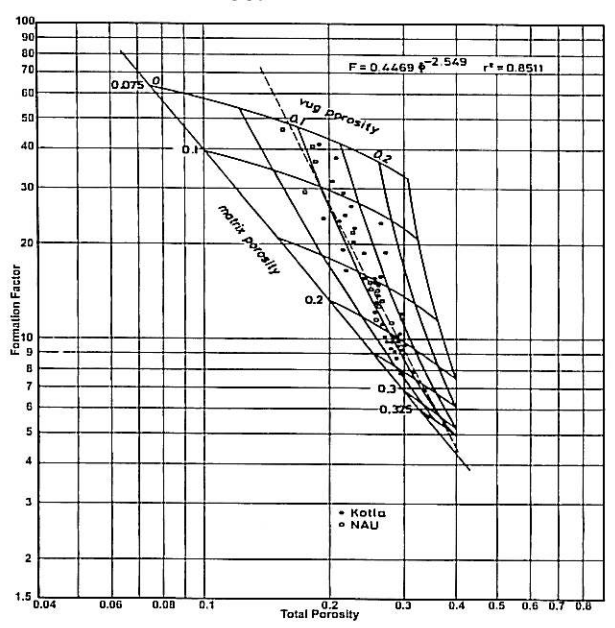


Fig. 2(a). Application of Maxwell-Garnett model to abundant interconnected touching and channel like vuggy porosity from skeletal and micritic matrix leaching, dominant on 1" and 1.5" small plug scale.

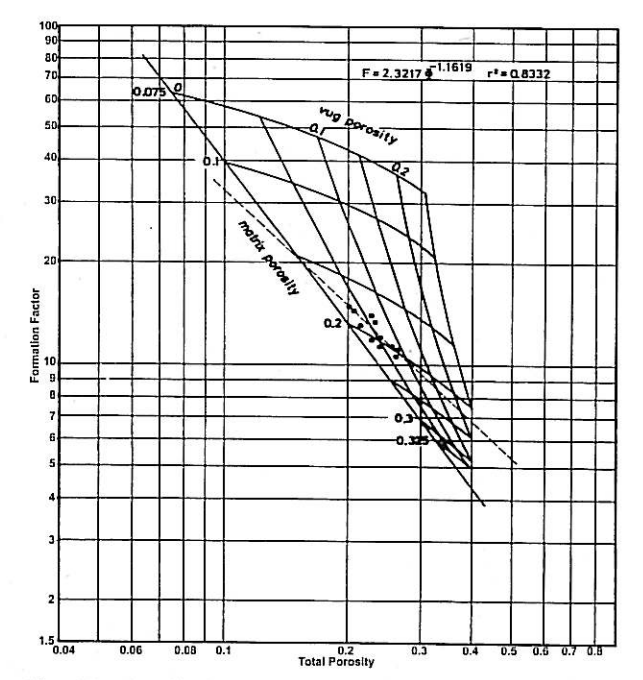


Fig. 2(b). Application of Maxwell-Garnett model to discrete, separate vuggy porosity, dominant on 1.5", full diameter and well log scale. Model allows division of total porosity into matrix and vuggy porosity components (from El-Ashahab, Krizmanic, Gherryo)[18,19].

For a elatively clean carbonate rock with a high salinity environment FF does not appear to be affected by surface conductance of clay component.

B.) Use of Maxwell-Garnet Model to Separate Total Porosity into Intergranular and Vuggy Pore Space.

Vuggy porosity is difficult to calculate from wireline logs, and requires detailed core-log calibration to give reasonable results. We separate total porosity into intergranular and vuggy porosity components, applying the M-G model [18,19]. The relations are:

$$\Phi_v = 0.8139 \Phi_t - 0.1353$$
 $r^2 = 0.7495$ (4) discrete vuggy system

$$\Phi_i = 0.0263e^{6.9401\Phi_i} \qquad r^2 = 0.7847 \tag{5}$$

abundant vuggy system

Thin-section image analysis provides a good approach of the effective vuggy porosity in carbonate rocks. Figure 3 shows comparison between vuggy versus total porosity from the M-G model, and from thin-section description of core material^[20].

The M-G model is efficient in separating total porosity into intergranular and secondary dissolution.

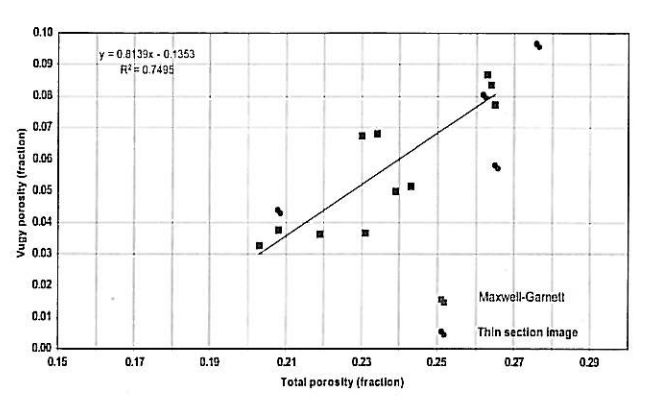


Fig. 3. Good agreement of vuggy vs. total porosity from thinsection analysis and from the Maxwell-Garnett model indicates usefulness of the model (from Krizmanic, Labedi, Abdulkarim, Gherryo) [18,19,20].

C.) Resistivity Index.

Laboratory resistivity measurements of FF and resistivity index, I_R , are acquired on rock samples to increase consistency of the log data interpretation. The evaluation of the amount and distribution of oil in place depend heavily on the model applied to describe links between FF, I_R and water saturation.

The resistivity index measurements were performed in conjunction with porous-plate, oil/brine capillary pressure. Sufficient time is allowed at each point for wattability restoration and equilibrium saturation to be achieved. A 4-electrode setting was used to avoid contact resistance and end effects^[14]. Table 1 shows the properties of sample used and formation brine.

Figure 4 shows resistivity index curves versus saturation. Mercury capillary pressure curves interpreted in terms of pore throat size distribution show uni-modal pore size distribution within intergranular pore space. Low saturation exponent (n), and departure of $I_{\rm p}$ versus

Table 1. Core sample petrophysical parameters, properties of formation brine and tests condition.

Ambient condition air permeability, mD	15.5	
NOB condition porosity, fraction	0.262	
Saturation exponent (n)	1.65	
Net overburden (NOB) pressure	3000	
Temperature, °F, (°C)	150, (66)	
Brine salinity, mg/l TDS	189 991	
Resistivity of brine, Ohm-m at 77°F	0.054	

S_w from ideal Archie's law recently have been paid attention, and have been experimentally documented and theoretically explained 21 through 26.

Two slopes could explain I_r versus S_w relation. The first shows the invading of the vuggy pore space by oil. Vuggy rock surface is rendered to be strongly oil wet. The second describes subsequent invasion of the intergranular pore space^[20]. Best fit of the second straight-line segment is:

$$I_r = 2.6731S_w^{-1.09}$$
 $r^2 = 0.9961$ (6)

The relation is valid in saturation range $0.78 < S_w > 0.099$. The change in the value of n at $S_w = 0.78$ provides the vuggy porosity component of

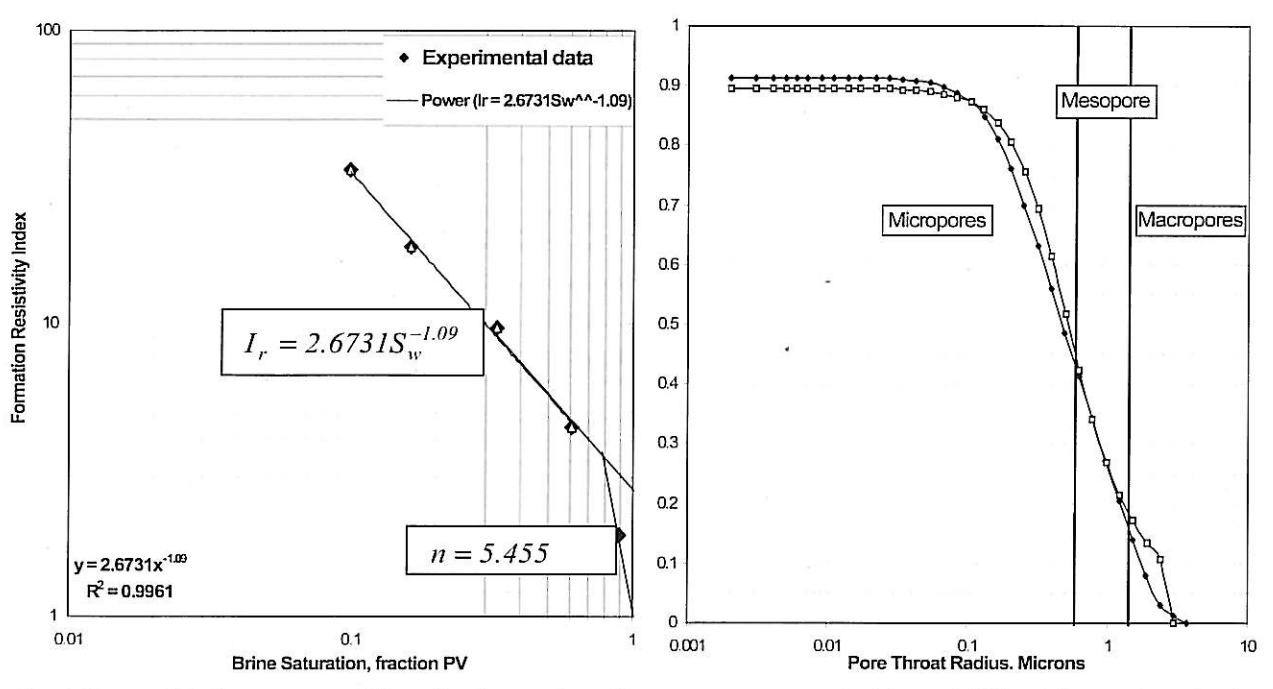


Fig. 4. Two straight-line segments of I_r vs. S_w : desaturation of vuggy pore space resulted in n = 5.455 and desaturation of unimodal interganular pore space resulted in $I_r = 2.673 IS_w^{1.09}$. Microporosity is linked to the presence of micrite crystals (from Gherryo Krizmanic, Labedi, Abdulkarim) I_r^{20} .

Φvug = 0.058, for the total sample porosity Φtot = 0.262. The oil content in vuggy pore space is S_{ov} = 0.22. The M-G model (4) provides vuggy porosity component of Φvug = 0.078, and S_{ov} = 0.292.

The second straight-line implies:

- a) Unimodal pore size distribution of the intergranular pore space, as indicated by the mercury injection data and
- b) There is no wettability induced change in electrical properties within intergranular pore space.

The wettability question in intergranular pore system may be the matter of some concern.

D) Water Saturation Model.

Use of coreflood test data to provides arguments for the choice of adequate saturation models. Checking the validity of different models, and calibration of the parameters remain a frequent problem in log interpretation^[23,25] through 29]. We modified Archie's model. The modified Archie's model is^[20]:

$$S_{w} = \left[\left(\frac{R_{w}}{R_{t}} \right) \frac{a}{b} \boldsymbol{\Phi}^{-m} \right]^{1/n} \tag{7}$$

where b comes from : $S_w = bI_r^{-n}$

The model: I_r =2.6731 S_w -1.09 provides model parameters b = 2.6731 and n = -1.09. Eq. (3) provides model parameters a = 2.3217 and m = -1.1619, while Eq. (4) provides model for separation of total porosity into discrete vuggy porosity component in total. These model parameters, coupled with gas-flood tests data, provide arguments that the selected saturation model is adequate.

For considered carbonate formations, Figure 5 shows vuggy oil saturation as a function of initial oil saturation, porosity and formation resistivity range.

Tables 2 and 3 show secondary CO_2 gravity drainage experimental data. Breakthrough, BT, of CO_2 occurred at 38.2% PVI, resulting in oil saturation reduction of $\Delta S_o = 0.271$. The M-G model provides vuggy oil saturation $S_{ov} = 0.292$. Evidently oil contained in intergranular pore space is not efficiently accessible to CO_2 with IFT = 2.7 mN/m.

Figure 6 shows comparison of vuggy porosity and oil content in vuggy pore space evaluated by: M-G models, resistivity index and displacement experimental tests. The Archie's water saturation model, conditioning to gas core-flood tests data, exhibits high consistency of all data.

Fig. 6. shows the comparison of vuggy porosity and vuggy oil saturation from M-G model, resistivity index, and displacement tests. Resitivity and coreflood tests provide arguments for the choice of adequate

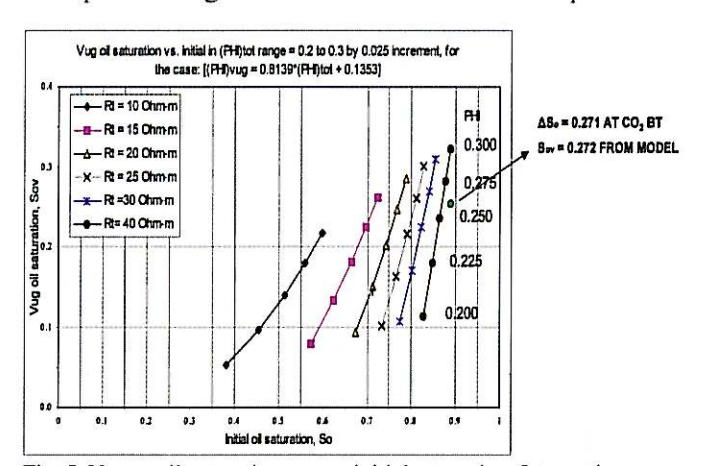


Fig. 5. Vuggy oil saturation versus initial saturation. Integration of $\rm I_R$ measurements with displacement test provide arguments for the choice of adequate saturation model.

Table 2. Long stacked core properties

Test	L(cm)	D (cm)	V (m/d)	Swi	Kw (mD)	Ko(Swi) (mD)	ф
Gravity stable	150	4.5	0.146	0.079	28		0.264
WAG	147	4.5	0.150	0.251	37	17	0.255

Table 3. Statistics of gravity stable and WAG secondary displacement tests.

@ water breakthrough				@ gas breakthrough					
	PVI (%)	R (%OOIP)	S _{oi}	S _o @BT	S _{oi} -S _o BT	PVI(%)	R(%OOIP)	S _o @BT	S _{oi} -S _o BT
Gr.			0.921			38.1	26.3	0.65	0.271
Dr.			0.521			50.1	20.5	0.02	0.271
WAG	62.66	63.46	0.749	0.272	0.477	88.16	73.8	0.202	0.547

	@ the end o	of continuous gas injec	tion			
	PVI (%)	Rfinal (%OOIP)	Soi	S _{or}	S _{oi} - S or	$S_{\rm gfinal}$
Gr. St	191.2	51.4	0.921	0.514	0.407	0.407
WAG	109.4	90.72	0.749	0.0769	0.6795	0.6721

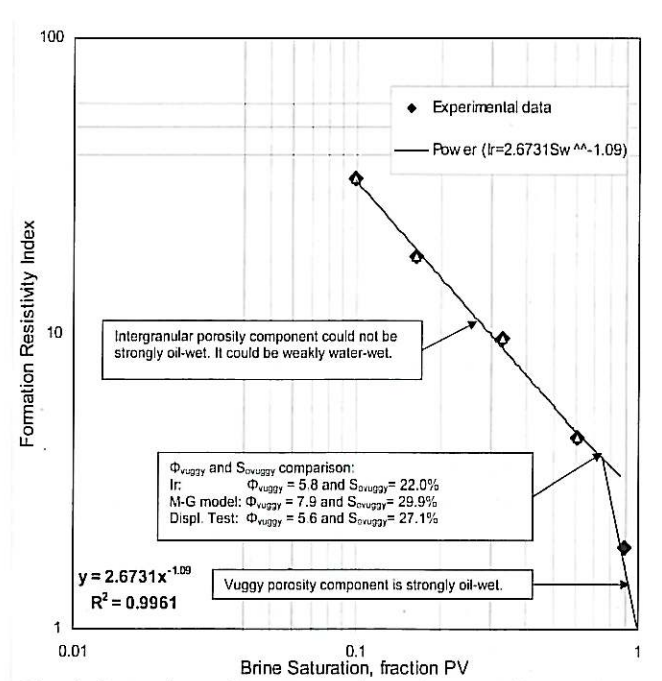


Fig. 6. Comparison of vuggy porosity and vuggy oil saturation from M-G model, resistivity index, and displacement tests. Resitivity and coreflood tests provide arguments for the choice of adequate interpretation model. (from Gherryo, Krizmanic, Labedi, Abdulkarim) ^[20].

interpretation model. (From Gherryo, Krizmanic, Labedi, Abdulkarim^[20]).

The model provides higher values for oil in place contained in mesopores and micropores of intergranular pore space, target for EOR technologies. It provides good estimates of both the vuggy porosity component in total and the oil content in vuggs.

CORE-FLOOD DISPLACEMENT TESTS

Petrophysical Characterization on Small Core Plugs.

The petrophysical characterization on small core plugs is essential for considering interpretation of the IWAG and gravity drainage experiments on long composite cores. The tests include:

- a) Mercury injection and pore throat size distribution analysis,
- b) Centrifuge oil/water drainage/imbibitions and gas/oil/connate water drainage capillary pressure curves the average saturations are corrected to obtain the saturations at inlet face of the plugs,
- c) Oil/water imbibitions relative permeability curves and gas/oil/connate water drainage relative perms and
 - d) IFT measurements on CO₂ swollen fluids.

The tests were performed on wettability restored 1.5 inches in diameter, and 2.5 to 3 inches in length plugs. The resulting two-phase relative permeability will be used to help interpretation of IWAG and gravity stable drainage displacement tests on long, stacked cores.

Research shows that the centrifuge method is a fast and reliable method for obtaining oil desaturation curve as a function of trapping number, NT, in regions of low oil relative permeability, and in reservoirs where gravity drainage controls the recovery process^[11,30] through ³⁴].

$$N_T = \frac{\left| K \left(\nabla P + g \Delta \rho \nabla D \right) \right|}{\sigma} \tag{8}$$

Figure 7 shows oil desaturation curves for twophase oil/water, and three-phase oil/gas/connate water systems. The advantage over displacement tests is evident.

Reservoir simulation requires a realistic spatial distribution of capillary pressure and relative permeability. Drainage capillary pressure curves are used to predict initial water saturation, while imbibitions capillary pressure curves significantly impacts overall displacement efficiency. Figures 8 a and b show oil/water and gas/oil/ connate water centrifuge capillary pressure curves.

Unsteady-state water-flood and gas-flood tests were carried out on restored state cores. Capillary pressure curves were used as an input for numerical calculation — which means that the residual oil

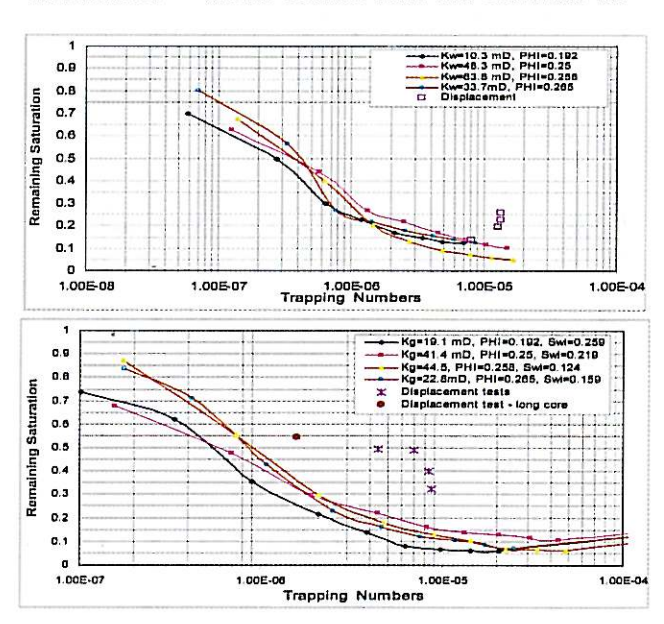


Fig. 7. Remaining oil saturation, S_{or} , achieved in displacement tests in comparison with oil de-saturation centrifuge capillary pressure curves: oil/water and oil/gas/connate water systems. Low S_{or} values are result of continuous oil film drainage.

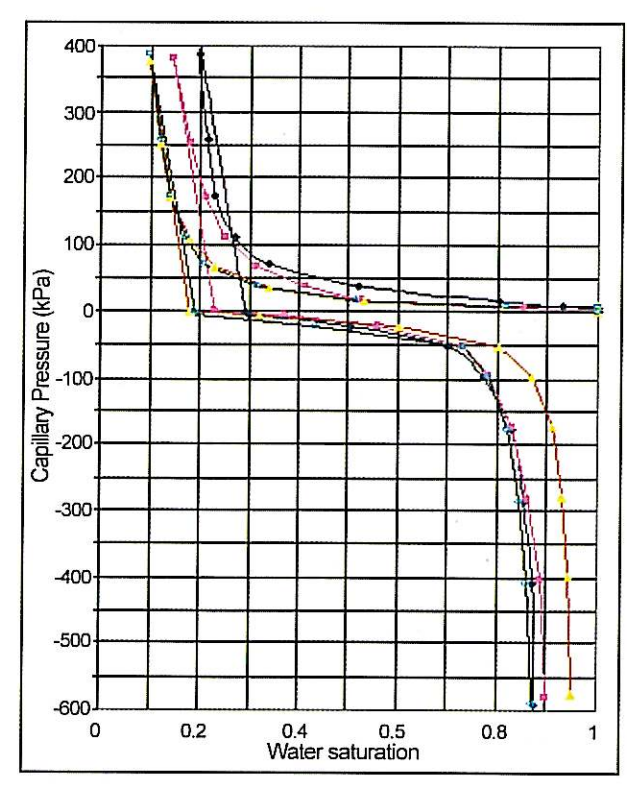


Fig. 8(a). Capillary pressure oil/water drainage/imbibitions curves – negative branches of Pc curves show that displacement efficiency could be deteriorated by strong capillary retention forces.

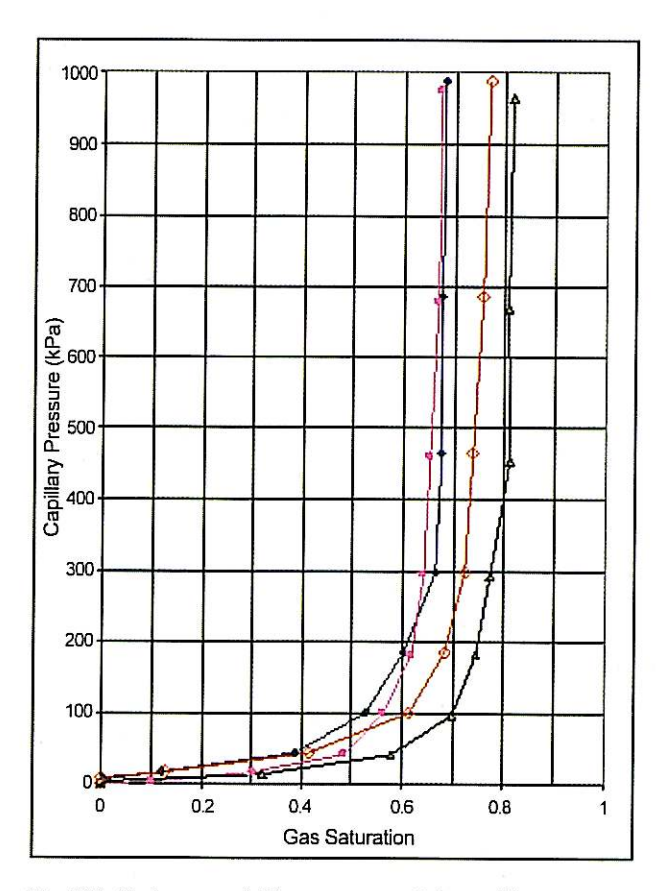


Fig. 8(b). Drainage gas/oil/connate water Pc's, capillary pressure curves were input in core-flood simulator.

saturations are supposed to be equal for displacement and centrifuge experiments. Therefore the relative permeability curves, obtained by history matching of production data with numerical coreflood simulator, take into account of viscous, capillary and gravity forces.

Figures 8 c and d show oil/water and gas/oil relative permeability curves. Although the oil could be displaced by oil-wetting layers to very low S_{or} values, the efficiency would be deteriorated by low

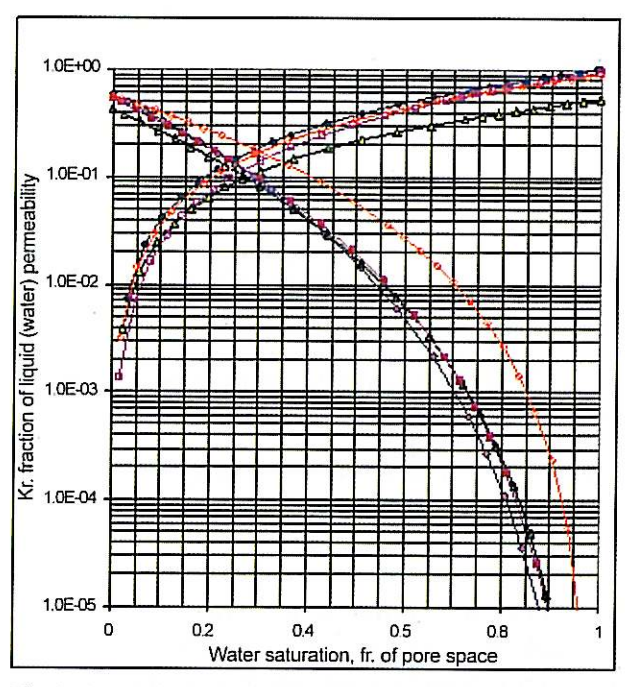


Fig. 8(c). Relative permeability curves oil/water.

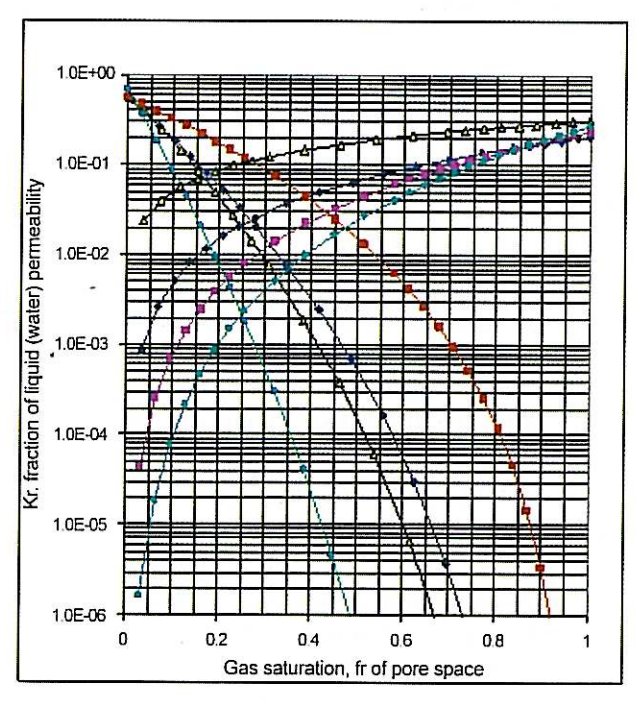


Fig. 8(d). Gas/oil relative permeability curves correctly account for viscous, capillary and gravity effects.

rates because relative permeability is also low in the range from 1E-3 up to 1E-5 and lower. Large scatter of oil/gas relative permeability curves is related to heterogeneity of small core-plugs.

Petrophysical characterization on small core plugs is an indispensable step for interpretation of displacement tests on long stacked cores.

Statistics of Secondary CO₂ Gravity Drainage and WAG Experiments on Long Stacked Cores.

Tests were performed at pressure of 193 barg. (MMP = 270 barg). Table 2 lists basic rock properties of long stacked cores. Dual energy x-ray detection allows assessing oil, water, and gas saturation profiles along the core.

Secondary CO₂ Gravity Drainage Experiment.

Table 3 shows statistics of the secondary gravity drainage and IWAG displacement tests. Final oil recovery R = 41.4% of OOIP, left behind residual oil saturation $S_{\rm org} = 0.544$. CO_2 BT occurred at 38.2% PVI, when oil recovery at gas BT is 26.3% of OOIP. Oil saturation reduction of $\Delta S_{\rm o} = 0.271$ is exactly the swept volume of oil contained in vuggy porosity space (The M-G model provides $S_{\rm ovug} = 0.292$). Evidently oil contained in intergranular pore space is not efficiently accessible to CO_2 with IFT = 2.7 mN/m. To access the oil contained in this pore space, a high reduction in IFT is needed. The reservoir pressure should be maintained at a level in excess of $P_r = 270$ bar.

The test was interpreted by numerical calculation to provide oil/gas relative permeability as an input for correct description of IWAG process on core scale.

Secondary IWAG Displacement Test was carried out with CO_2 injected first, followed by water. The slug sizes were approximately 8.4% PV. The IWAG injection resulted in final oil recovery, $R_i = 90.7\%$ of the OOIP with left behind residual oil saturation, $S_{or} = 0.0769$. Water broke through first resulting in oil recovery, $R_{wbt} = 63.5\%$ of OOIP, followed by gas BT with an oil recovery of $R_{gbt} = 73.8\%$ of OOIP.

The IWAG process is more efficient than secondary gravity drainage. From core scale point of view the IWAG technology could be the right technology for carbonate reservoirs of identical depositional environment and fabric-selective dissolution process. The process is immiscible and it could potentially: a) recover the same amount of oil

as the miscible process with CO₂, but at a significantly lower pressure, b) work well using the other gases, and c) work well at even lower reservoir pressures.

Pore scale and core scale displacement scenario. In vuggy porosity space, oil is a strongly wetted phase retaining continuity even at low oil saturation based on SCAL tests results. Water is a non-wetted phase. Gas is a wetting phase relative to water. Neither gas in presence of water, nor water in presence of gas, could spread on oil forming continuous gas or water films.

The first gas injection cycle.

Gas displaced oil from the largest oil-wet vuggy pore space by piston like displacement, and through continuous oil film drainage.

The first water injection cycle.

Water displaced gas and oil from the largest oilwet vuggy pore space by double displacement. Gas had been displaced by piston-like and, oil through continuous wetting oil film flow. Due to adverse mobility ratio, gas had channeled through the oil occupied pores forming an oil bank ahead of water. As a result of capillary competition between gas and oil and gas and water, snap-off of gas and trapping could occur only by oil in the gas occupied pores.

Gas snap-off by water and gas trapping could not be possible in water invading zone. However in this zone, gas could be bypassed in larger oil-wet pores.

In intergranular pore space, wettability was randomly distributed to a degree of $COS\Theta_{ow}$ for each pore size. Larger pores preferentially oil wet, were surrounded by smaller preferentially water-wet pores. Water had invaded the smallest weakly-water to weakly-oil wet pores by capillary diffusion. From this pore network, oil could be displaced by a corner filaments flow and by a piston like displacement depending upon wettability and water/oil contact angle hysteresis [5,33,34].

As a consequence of this capillary dominated flow, feeding and thickening of oil films in larger oil-wet pores of vuggy pore space occurred. Oil bank ahead water-front increased in size through oil film flow, and more gas was trapped by snap-off and bypassing. Trapped and bypassed gas reduced mobility of advancing water-front and formed oil bank, which resulted in a steady increase of water injection pressure.

Increase of water injection pressure favored a capillary controlled water flow into the smallest pore network and forced (viscous) controlled into the largest pore network of intergranular pore space. Viscous flow of water from vuggy to intergranular pore space has been initiated when the water pressure in vuggy pore space, P_w , exceeded oil pressure in integranular, P_o by capillary entry pressure given by $(s_{ow} cos\Theta_{ow})/r$. For largest preferentially oil-wet intergranular pores, $-1 \le cos\Theta_{ow} \le 0$. Oil which squeezed into vuggy pore space supported flow of continuous oil films, and made oil bank increased in size trapping more gas.

Trapped gas could be remobilized by dissolving in water and oil and by compression. At some threshold pressure, compressed trapped gas globules collapsed and/or were squeezed ahead, forming a small gas bank of free gas saturation within oil bank. Compression/decompression of trapped gas added to increased/decreased oscillations of injection pressure. Figure 9 shows oscillations of injection pressure for the first and second water injection cycles.

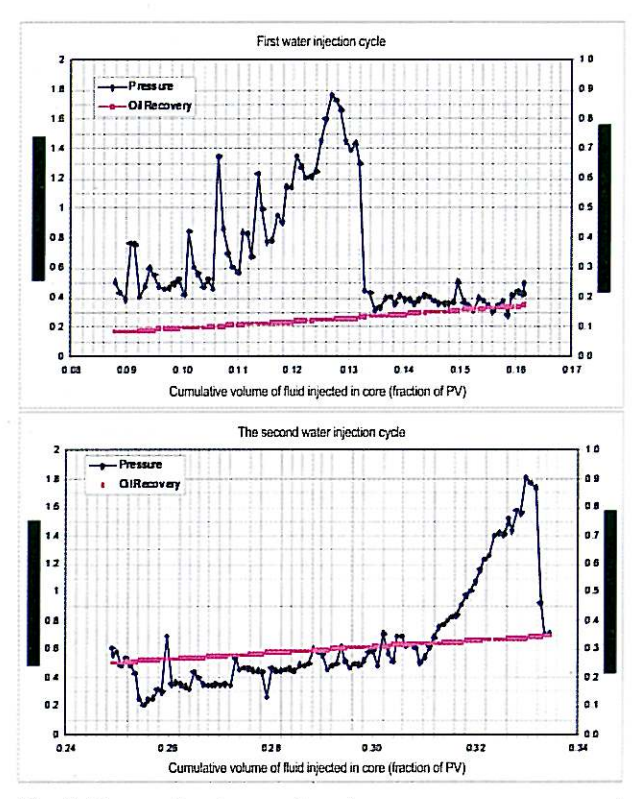


Fig. 9. Bypassed and trapped gas in vuggy pore space caused increase of water injectivity. Pressure increase favored spontaneous and forced imbibitions of water from vuggy into intergranular pore space and countercurrent flow of oil into vuggy pore space. More gas was trapped in formed oil bank. Collapse of trapped gas resulted in a sudden decrease of injection pressure and forming free gas bank ahead of formed oil bank.

Subsequent gas injection cycles.

Since for strongly oil-wet vuggy pore network, $-1 \le cos\Theta_{gw} \le 0$ and $0 < cos\Theta_{go} \le 1$, or $(\sigma_{go}cos\Theta_{go}) \ge (\sigma_{gw}cos\Theta_{gw})$ gas preferred to enter the water filled pores of strongly oil-wet vuggy pore network. In the first injection cycle, injection pressure was higher when gas displaced oil and injection pressure became almost zero, or even small minus when gas displaced water from pores previously occupied by oil. This indicates that gas was a wetting phase relative to water in the strongly oil-wet vuggy pore space.

Water has been displaced by a piston-like displacement, and oil by a continuous oil films drainage. This means that water could become disconnected phase.

Due to the reduced mobility of water-front and oil bank, gas injection pressure had increased. Gas was forced to penetrate from vuggy into intergranular pore space. Gas could be either wetting or non-wetting phase relative to water, depending upon randomly distributed wettability for each pore size and non-wetting relative to oil. Gas occupancy preference of pore space is given by the relations between wettability, IFT, and pore size: $(\sigma_{go}cos\Theta_{go})/r$, and $(\sigma_{gw}cos\Theta_{gw})/r$. Gas preferred to occupy the largest pores filled by water from previous water injection cycle. Then, when faced with pores of equal radius, gas preferred to enter pores filled with oil, as the IFT between gas and oil was lower than between gas and water.

The process caused feeding the vuggy pore space by oil and redistribution of oil, gas and water in the intergranular pore space. Due to the redistribution of fluids and gas compression, the gas cycles were inefficient in oil recovery. Figure 10 shows that these features are common in gas injection cycles.

Subsequent water injection cycles.

Water invaded the smallest water-wet pores by capillary diffusion and displaced gas and oil from previously gas filled pores by double displacement process because of wetting and spreading conditions. Oil expelled from intergarnular pore space has increased thickness of continuous oil films in oil-wet vugyy pore network, which had been efficiently drained to the formed oil bank ahead waterfront.

As a result of multiple displacements gas had been squeezed from the largest to the next to largest, oil saturated pores. Therefore gas could be trapped since

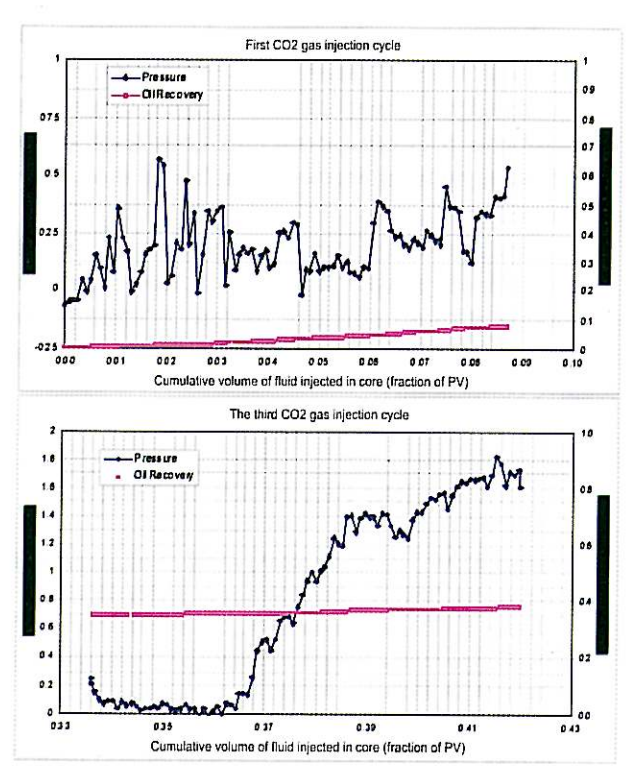


Fig. 10. Gas displaced water and oil from the largest vuggy pore space. Mobility increase in water-front and oil banks in vuggy pore space increase gas injectivity. Gas was forced to occupy the largest water and oil filled pores, squeezing oil into vuggy pore space. Gas was trapped in intergranular pore space by redistribution of phases in randomly distributed wettability for each pore size.

water became wetting to gas in the more weakly oilwet pores. It is also expected that gas could be bypassed in relatively larger pores as these pores were surrounded by smaller, water wetting pore throats, from which water could not be displaced by gas.

Obviously continuity of oil wetting films in both pore networks made this process extremely efficient in oil recovery on scales of pores and core scale.

Cycling of gas and water injection resulted in an increasing-decreasing oscillation in the injection pressure. Therefore within leading oil bank, gas saturation consisted of trapped gas and formed slugs of free gas saturation. The gas production profiles in Figure 11 show that the slugs of free gas were produced before and after water breakthrough. Oil expelled from intergranular pore space was efficiently drained through the increased thickness of continuous oil films.

Additional 10% of oil was produced between water breakthrough and followed gas breakthrough. Large quantity of gas had been retained efficiently in intergranular pore network of randomly distributed wettability for each pore size.

Water saturation model provides higher values for oil in place contained in mesopores and micropores of

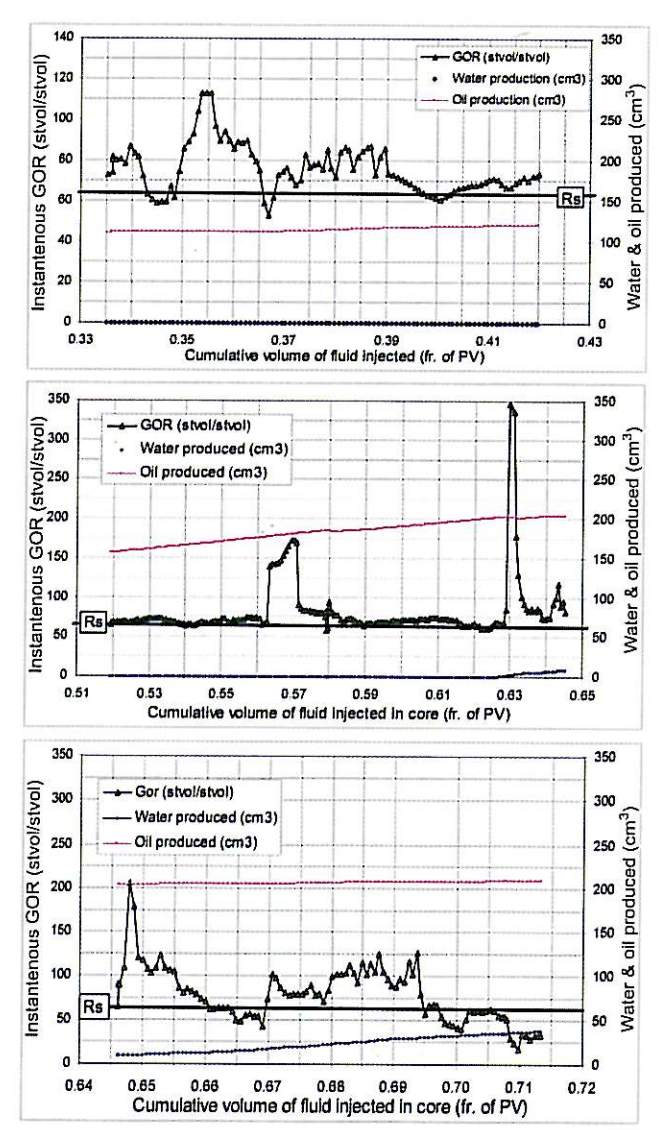


Fig. 11. Banks of free gas produced ahead of gas breakthrough suggested efficient oil expelling from intergranular pore space into vuggy by water and gas invasion. 10% of oil recovered between water and gas breakthroughs suggested efficient oil film flow in vuggy and intrgranular pore space and efficient gas trapping and blockages in intergranular pore network of randomly distributed wettability for each pore size.

intergranular pore space target for EOR technologies. From this point of view, IWAG process could be economically attractive. However the question is: could IWAG efficiently recover oil contained in intergranular pore space on large field scale application?

CAN WE EXPECT IWAG INJECTIVITY ABNORMALITIES AND EXTEND THREEPHASE IWAG PHENOMENA THROUGHOUT RESERVOIR IN THE FIELD APPLICATION?

Well-documented three-phase phenomena can

lead to abnormal injectivity losses in IWAG processes. Substantial loss in water and gas injectivity observed on core scale could potentially increase the injection pressure, adding additional injection wells in the field application. Reduction of water and gas relative permeabilities from a situation when only water and oil phases flow, to the situation where flows of water, oil and gas are present, is important to consider for the IWAG injectivity abnormalities, pressure profiles within reservoir, and breakthrough of water. IWAG efficiency could be restricted in the reservoir volume around injection wells, where most of three-phase phenomena would occur, potentially reducing benefit of IWAG efficiency on the scale of field.

Therefore to predict IWAG behavior in the reservoir from experimental displacement results, a numerical simulation with an effective hysteresis description of three phase (oil, water and gas) relative permeability should be developed.

CONCLUSIONS

- 1. The technological research, experimental and simulation studies are prerequisites for selecting the right technologies for IOR. The integration of SCAL and core-flood tests results supports implementation of IWAG technology in a number of carbonate reservoirs of identical depositional environment and selective fabric-dissolution process. The process is immiscible and it could potentially work well with any other immiscible gases, at a significantly lower pressure than required MMP.
- 2. Further theoretical, experimental and simulation studies are required to provide technological and economical feasibility such as: selecting the right technology for the reservoirs, the amount of increased hydrocarbon reserves on field scale and reduction in unit production costs and initial developments of maturing oil fields.
- 3. To achieve these goals, the reservoir must be characterized from a variety of viewpoints with a large number of parameters and with remarkable degree of accuracy and consistency. All information should be gathered and integrated to reduce uncertainty, improve efficiency and help to select the right technology for selected reservoirs.
- 4. Tree-phase phenomena could lead to abnormal high injectivity losses in WAG process. Increasing the injection pressure, adding additional injection wells, and IWAG efficiency restriction in the reservoir volume around injection wells, where most of three-

phase phenomena would occur, would potentially add difficulties to apply IWAG successfully in fields. Therefore a development of realistic cycle-dependent three-phase relative permeability model from coreflood tests by numerical simulation should be performed.

5. Design of IWAG process by simulation should include three-phase flow description through development of an effective hysteresis description of three-phase, cycle-dependent oil, water and gas relative permeability.

REFERENCES

- [1] Green, D.W., Willhite, G.P., 1998. Enhanced Oil Recovery. SPE Textbook Series 6, Richardson, TX.
- [2] Huang, E.T.S., and Holm, L.W., 1988 (Feb.). Effect of WAG injection and rock wettability on oil recovery during CO, flooding. SPERE.
- [3] Lin.E.C., and Huang, E.T.S., 1990 (May). The effect of rock wettability on water blocking during miscible displacement. SPERE..
- [4] Schneider, F.N., Owens, W.W., 1976 (Feb.). Relative permeability studies of gas-water flow following solvent injection in carbonate rocks. SPEJ.
- [5] Kralik, J.G., Manak, L.J., Jerauld, G.R., and Spence, A.P., 2000 (Oct.). Effect of trapped gas on relative permeability and residual oil saturation in an oil-wet sandstone. SPE 62997 presented at the 2000 SPE ATCE, Dallas, TX.
- [6] Krizmanic, K. El-Ashahab, B., Abdelkarim, O. and El-Fakhri, S., 2001 (Nov.) Trapped gas saturation – interpretation of experimental data for considering immiscible and miscible WAG injection." Nafta (Zagrb-Croatia).
- [7] Skague, A., 1996 (Sept.). Influence of wettability on trapped nonwetting phase saturation in three-phase flow. Procedings 4th International Symposium on Wettability and its' Effect on Oil Recovery, Montpelier, France.
- [8] Larsen, J.A., Skague, A., 1998 (June). Methodology for Numerical Simulation With cyclic-Dependent Relative Permeabilities. SPE Journal.
- [9] Larsen, J., A., Skague, A., 2000 (Oct.). Simulation of the immiscible WAG process using cycle-dependent three-phase relative permeabilities. SPE 56475 presented at the 1999 SPE ATCE, Houston, TX.
- [10] Christie, M.A., Muggeridge, A.H., Barley, J.J., 1993 (Feb.). 3D simulation of viscous fingering and WAG schemes. SPE Reservoir Evaluation.
- [11] Abdelkarim, O., Krizmanic, K., El-Ashahab, B., El-Fakhri, S. and Nesmari, N, 2001 (June). Some aspects of CO₂ flood for Sirte Basin reservoirs (Libya). OAPEC_IFP Joint Seminar, Paris, France.

- [12] Abdelkarim, O., El-Fakhri, S. Krizmanic, K., and Nesmari, N., 1999 (Nov.). An overview of CO₂ flood projects in the Arabian Gulf Oil Company. The 6th Mediterranean Petroleum Conference and Exhibition, Tripoli, Libya.
- [13] Krizmanic, K., Abdelkarim, O., El-Fakhri, S. and Nesmari, N., and El-Ashahab, B., 2000 (July). CO₂ flood projects of clastic and carbonate reservoirs in The Arabian Gulf Oil Company - Libya. Nafta (Zagrb-Croatia).
- [14] Core Laboratories: Advanced Rock Properties Study for the AGOCO. March 1998 through July, 2002.
- [15] TOTAL, 1998 (Oct.). Nafoora Augila field long composite cores and reservoir fluid characterization.
- [16] Maxwell-Garnett, J.C., Transaction of the Royal Society, London, 203, 385.
- [17] Herrick, D.C., and Kennedy, W.D., 1995 (June). Formation resistivity factor and permeability relationships in rocks characterized by secondary solution porosity. Paper QQQ presented at SPWLA 36th Annual Logging Symp., Paris.
- [18] Krizmanic, K., El-Ashahab, B.M., and Gherryo, J., 2000 (Aug.). Kotla and Nafoora Augila Unit – Formation Resistivity Factor Analysis. AGOCO internal documentation.
- [19] El-Ashahab, B.M., Krizmanic, K., and Gherryo, J., 2002 (July). Formation resistivity factor for carbonate reservoirs – Sirte Basin, Libya. Nafta.
- [20] Gherryo, J.S, Krizmanic, K., Labedi, R., Abdulkarim, O., 2004 (Jan.). Integration resistivity, pore size distribution and core-flood displacement tests provides arguments for the choice of adequate saturation model in rock characterized by solution porosity. Paper presented the 8th Mediterranean Petroleum Conference & Exhibition, Tripoli, Libya.
- [21] Swanson, B.F., 1985 (June). Microporosity in reservoir rocks. its measurement and influence on electrical resistivity. Paper F presented at the 1985 SPWLA Annual Logging Symposium, Dallas.
- [22] Wortington, P.F., Pallat, N., and Toussaint-Jackson, J.E., 1989 (June). Influence of microporosity on the evaluation of hydrocarbon saturation. SPE Formation Evaluation.
- [23] Argaud, M., Giouse, H., Starley, C., Tomanic, J., and Winkler, K., 1989 (Oct.). Salinity and saturation effects on shaly sandstone conductivity. Paper SPE 19577 presented at 1989 SPE ATCE, San Antonio, TX.
- [24] Wortington, P.F., and Pallat, N., 1992 (June). Effect of variable saturation exponent on the evaluation of hydrocarbon saturation. SPE Formation Evaluation.

- [25] Krizmanic, K., Mesmari, N., Obeida, T.A., and El-Ashahab, B.M., 1997 (July). The effect of variable saturation exponent on original oil in place evaluation –Sarir sandstone case, Libya. Nafta, 48.
- [26] Claudine, C., Brosee, E., and Cerepi, A., 2001 (June). Effect of pore-lining chlorite on petrophysical properties of low-resistivity sandstone reservoirs. SPE Reservoir Evaluation & Engineering.
- [27] Waxman, M.H., and Smiths, L.J.M., 1968 (June). Electrical conductivities in oil-bearing shaly sands. *SPEJ*.
- [28] Waxman, M.H., and Thomas, E.C., 1974 (Feb.). Electrical conductivities in shaly sands -I. The temperature coefficient of electrical conductivity. *JPT*.
- [29] Clavier, C., Coates, G., and Dumanoir, J., 1977 (Oct.). The theoretical and experimental bases for 'dual water' model for the interpretation of shaly sands. Paper SPE 6859 presented at 1977 SPE ATCE, Denver, Colorado.
- [30] Hirasaki, G.J., 1995 (Oct.). Dependence of waterflood remaining oil saturation on relative permeability, capillary pressure and reservoir parameters in mixedwet, turbidite sands. Paper SPE 30076 presented at 1995 SPE ATCE, Dallas, TX.
- [31] Sharma, M.M., and Filoco, P.R., 2000 (Sept.). Effect of brine salinity and crude-oil properties on oil recovery and residual saturations. *SPE Journal*.
- [32] Jain, V., Chattopadhyay, S., and Sharma, M.M., 2002 (April). Effect of capillary pressure, salinity, and aging on wettability alteration in sandstones and limestones. Paper SPE 75189 presented at the 2002 SPE/DOE IOR Symp., Tulsa, OK.
- [33] Sohrabi, M., Henderson, G. D., Tehrani, D.H., Danesh, A., 2000 (Oct.). Visualisation of oil recovery by water alternating gas (WAG) injection using high pressure micromodels – water-wet system. Paper SPE 63000 presented at 2000 SPE Annual Technical Conference and Exhibition, Dallas, TX.
- [34] van Dijke, M.I.J., Sorbi, K.S., Sohrabi, M., Tehrani, D.H., Danesh, A., 2002 (April). Three-phase flow in WAG process in mixed-wet porous media: pore-scale network simulations and comparison with micromodel experiments. Paper SPE 75192 presented at the 2002 SPE/DOE Improved Oil Recovery Symposium, Tulsa, OK.